

# AN ADJOINT-BASED OPTIMIZATION METHOD FOR HELICOPTER FUSELAGE BACKDOOR GEOMETRY

Q. Zhang, J.-D. Lee, J.-H. Wendisch

Institute for Aerodynamics and Flow Technology  
German Aerospace Center (DLR)  
Lilienthalplatz 7, 38108 Braunschweig, Germany  
E-mail: qinyin.zhang@dlr.de

## ABSTRACT

For utility and transport helicopters with rear loading backdoors, the afterbody area is usually one of the largest drag contributing areas of the fuselage. For this reason, numerical simulations have been performed to assess the possibilities of fuselage drag reduction by the means of local shape modification at the afterbody region. Within this study an automatic optimization chain with gradient-based optimization technique and surface parameterization/deformation tools has been established and applied to the backdoor geometry of a modified GOAHEAD configuration [1]. This paper will present the first numerical results of the ongoing shape optimization studies. As it turns out, local shape modification on the backdoor geometry can lead to a reduction of the separation region there and to a drag reduction of the helicopter fuselage.

## NOMENCLATURE

$C_D$	drag coefficient
$C_f$	skin friction coefficient
$C_L$	lift coefficient
$C_p$	pressure coefficient
$D$	design variables
$I$	cost function
$L$	Lagrangian function
$Ma$	Mach number
$p$	pressure
$R$	residual of the flow simulation
$Re$	Reynolds number per unit length, 1/m
$T$	temperature
$U$	velocity
$W$	flow variables
$X$	computational mesh
$\alpha$	angle of attack [°]
$\beta$	sideslip angle [°]
$\rho$	fluid density
$\Lambda$	Lagrangian multiplier

## ACRONYMS

CAD	Computer Aided Design
CFD	Computational Fluid Dynamics
DLR	Deutsches Zentrum für Luft- und Raumfahrt e. V.
GOAHEAD	Generation of Advanced Helicopter Experimental Aerodynamic Database for CFD code validation
GRC	Green Rotorcraft
ISA	International Standard Atmosphere
JTI	Joint Technology Initiative
NURBS	Non-Uniform Rational B-Splines
RANS	Reynolds Averaged Navier-Stokes
RBF	Radial Basis Function

## 1. INTRODUCTION

As the largest airframe component, the fuselage has a significant impact on the aerodynamic characteristics and performance of a helicopter. Especially in high-speed forward flight, the fuselage drag of helicopters is a major source of the overall aerodynamic drag. For a typical single-rotor helicopter under cruise flight condition at 150 knots,

the breakdown of power requirement has shown that over 45% of the total power is used to overcome airframe drag [2]. In particular for utility and transport helicopters, which feature upswept tails with backdoors to enable rear loading, one of the largest drag contributing areas of the basic fuselage was found to be the helicopter afterbody. The reasons for this effect are the appearance of flow separation and the formation of two strong trailing vortices in the afterbody region. Due to the mission design

requirement many parameters, like the upsweep angle or the contraction ratios of the afterbody, can not be modified, therefore, the local optimization of the afterbody shape is considered to be a promising approach to reduce the overall helicopter drag under high-speed flight conditions.

With the increasing computational power, the CFD has become a routine tool used for aerodynamic analysis and provides reasonably accurate results. However, the ultimate goal in the design process is to find the optimum shape which maximizes the aerodynamic performance. In optimum aerodynamic shape design problem with gradient-based optimization technique, one requires  $N+1$  flow evaluations for  $N$  design variables if forward-difference is used to calculate the required gradient information and this directly results in a severe increase in the computational time for each design cycle if high-fidelity code, e.g. Navier-Stokes, is used. Another approach which was first proposed by Jameson [3] is to treat the design problem as a control problem and has been proved to be very effective in wing shape optimization [4]. The wing is hereafter treated as a device which controls the flow to produce lift with minimum drag, and the theory of optimum control of systems can be applied. By adopting the governing partial differential equations of the optimum control theory, one can find the derivative of the cost function with respect to the shape by solving an adjoint equation problem. The total cost, which is nearly independent of number of design parameters, is one flow plus one adjoint evaluation and this makes this technique very promising for the optimum shape design. At the DLR, a solver for the discrete variant of the adjoint equation has been implemented into the unstructured RANS solver TAU code in the past [5], and it has been successfully applied to complex 3D wing and fuselage optimization problems [6].

In the current study, the discrete adjoint solver is adopted for the gradient calculation, and the optimization algorithm used is the conjugate-gradient method. The backdoor geometry, which is to be optimized within this study, is parameterized using an approximated NURBS surface, and the control points of the NURBS surface are the design variables of the optimization problem. The local shape modification of the backdoor geometry according to the directives of the optimizer is introduced into the CFD mesh via a mesh deformation method based on radial basis functions (RBF), which has been developed in the past for the purpose of fluid-structure coupling [7]. The applied numerical methods will be elucidated in the following section.

## 2. NUMERICAL METHODS

The automatic optimization chain for the fuselage drag reduction established in this study consists of the following ingredients: a CFD solver, a solver for the adjoint equations, surface parameterization and deformation tools. These components are combined together with a Python script, in which the optimum search is performed via a conjugate-gradient approach. An overview of the process chain is given in Figure 1. The computational intensive parts of the optimization chain are marked with yellow, and mesh deformations are performed in the green marked positions.

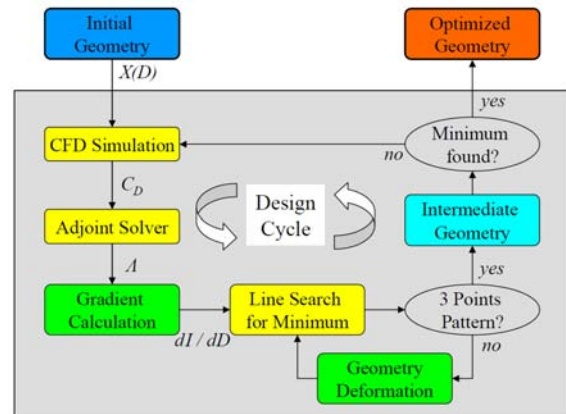


Figure 1: Optimization chain for the fuselage drag reduction.

### 2.1. CFD Solver TAU

The CFD code TAU is an unstructured compressible RANS solver based on a cell-vertex finite volume discretization which exploits the advantages of hybrid grids. In the current study, a central scheme of second order accuracy using Jameson-type of artificial dissipation is applied for the spatial discretization of the RANS equations. The time integration is performed with an implicit LUSGS scheme. Turbulence effects are taken into account by the Spalart-Allmaras model [8], which is a one-equation eddy viscosity model particularly suited for aeronautical aerodynamics. A speed-up of the computations is achieved by the multigrid technique. For more details of the TAU code the reader is referred to [9][10].

### 2.2. Discrete Adjoint Formulation

As mentioned in the introduction, employing the adjoint method allows the use of many design variables and still be able to evaluate the gradient

information in an affordable time. In the following, the basic formulation of the adjoint method will be described shortly. Further details concerning the implementation and applications can be found for instance in [5] and [6].

The gradient of a cost function  $I = I(W, X(D))$  (such as drag) with respect to a vector of design variables  $D$  is

$$\frac{dI}{dD} = \frac{\partial I}{\partial X} \frac{dX}{dD} + \frac{\partial I}{\partial W} \frac{dW}{dD}, \quad (1)$$

where  $X(D)$  is the computational mesh and  $W(D)$  the vector of flow variables. The term  $dW/dD$  is expensive to evaluate for a geometry that is parameterized by a large number of design variables. To eliminate this term, one can define a Lagrangian function  $L$  as

$$L = I + \Lambda^T R, \quad (2)$$

where  $R = R(W, X(D))$  is the flow residual and  $\Lambda$  is the Lagrangian multiplier. By applying the chain rule, the gradient of the Lagrangian function can be written as

$$\frac{dL}{dD} = \left[ \frac{\partial I}{\partial X} \frac{dX}{dD} + \frac{\partial I}{\partial W} \frac{dW}{dD} \right] + \Lambda^T \left[ \frac{\partial R}{\partial X} \frac{dX}{dD} + \frac{\partial R}{\partial W} \frac{dW}{dD} \right]. \quad (3)$$

After collecting terms between  $dX/dD$  and  $dW/dD$ , the gradient of Lagrangian can be represented as

$$\frac{dL}{dD} = \left[ \frac{\partial I}{\partial X} + \Lambda^T \frac{\partial R}{\partial D} \right] \frac{dX}{dD} + \left[ \frac{\partial I}{\partial W} + \Lambda^T \frac{\partial R}{\partial W} \right] \frac{dW}{dD} \quad (4)$$

If we set  $\Lambda$  to satisfy the adjoint equation

$$\left[ \frac{\partial R}{\partial W} \right]^T \Lambda = - \left[ \frac{\partial I}{\partial W} \right]^T, \quad (5)$$

the dependence of flow solutions on design variables,  $dW/dD$ , is eliminated and the evaluation of gradient reduces to

$$\frac{dI}{dD} = \frac{dL}{dD} = \left[ \frac{\partial I}{\partial X} + \Lambda^T \frac{\partial R}{\partial X} \right] \frac{dX}{dD}, \quad (6)$$

where the terms  $(\partial I / \partial X)(dX / dD)$  and  $(\partial R / \partial X)(dX / dD)$  can be cheaply evaluated with finite differences.

## 2.3. Optimization Algorithms

General gradient-based optimization involves the calculation of gradients and line searches along the direction. If we let  $x_k$  be the current design point corresponding to the  $k_{th}$  design iteration, the basic idea is to choose a downhill direction  $d_k$  and step size  $\alpha_s$  such that

$$I(x_k + \alpha_s d_k) \leq I(x_k) \quad (7)$$

is satisfied. In the steepest descent method, the search direction  $d_k$  is chosen to be the negative of the gradient at each iteration:

$$d_k = -\nabla I(x_k). \quad (8)$$

The conjugate gradient methods, which were first proposed by Fletcher and Reeves [11], are a dramatic improvement over the steepest descent method. The descent direction is defined as

$$d_{k+1} = -g_{k+1} + \beta_k d_k, \quad (9)$$

where  $g_{k+1}$  is the gradient at current step and  $d_k$  is the descent direction from previous step. This represent a deflection in the steepest descent direction and, in Fletcher-Reeves version,  $\beta_k$  is defined as

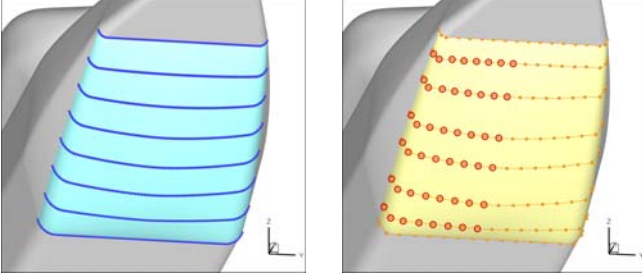
$$\beta_k = \frac{g_{k+1}^T g_{k+1}}{g_k^T g_k}. \quad (10)$$

After that a direction vector  $d_k$  has been chosen at current design iteration, the next step is to determine the step size  $\alpha_s$  along  $d_k$ , which corresponds a one-dimensional minimization problem. To minimize the cost, a bracketing algorithm is implemented and the optimum step size  $\alpha^*$  is trapped in a three-point pattern.

## 2.4. Surface Parameterization and Deformation

Since the objective of the current study is drag reduction by the means of local shape modification, only the backdoor area will be deformed. In general, the backdoor geometry of a helicopter can not be represented by simple 3D geometries. The NURBS surface parameterization technique is frequently

used in industrial design process, and it is able to represent complex shapes. Nevertheless, in the context of shape optimization, one of the disadvantages of the NURBS parameterization is that usually a large number of design parameters are needed for the geometrical description. To account for this effect, the adjoint-based optimization method was chosen for the current optimization method, in which the number of the design parameters plays a less important role for the gradient calculation.



(a) Original geometry (cyan) (b) Approximated NURBS Surface (yellow)

Figure 2: Approximation and reconstruction of the original backdoor surface geometry.

The basic idea of the NURBS parameterization is to split a curve or surface into piecewise polynomial or rational segments and to connect them with a prescribed level of continuity. For the purpose of the surface parameterization the original backdoor surface (the cyan surface in Figure 2a), is first cut at 8 different x-positions. The points along the cuts with the original geometry information (the blue points in Figure 2a) are used to generate NURBS curves. In general, a NURBS curve  $C(u)$  is defined by:

$$C(u) = \frac{\sum_{i=0}^n N_{i,p}(u) w_i \mathbf{d}_i}{\sum_{i=0}^n N_{i,p}(u) w_i} \quad 0 \leq u \leq 1. \quad (11)$$

This  $p_{\text{th}}$ -degree curve consists of the control points  $\mathbf{d}_i$  with their corresponding weights  $w_i$  and the  $p_{\text{th}}$ -degree B-Spline basis functions. The basis functions are calculated by a recurrence formula from Cox-de Boor [12]:

$$N_{i,0}(u) = \begin{cases} 1 & \text{for } u_i \leq u < u_{i+1} \\ 0 & \text{otherwise} \end{cases} \quad (12)$$

$$N_{i,p}(u) = \frac{u - u_i}{u_{i+p} - u_i} N_{i,p-1}(u) + \frac{u_{i+p+1} - u}{u_{i+p+1} - u_{i+1}} N_{i+1,p-1}(u)$$

An intrinsic optimization method from Hoschek [13]

has been implemented to improve the approximation accuracy of the NURBS curves.

A NURBS surface is a bivariate function with two parameters  $u$  and  $v$ . A tensor product scheme is a common method to describe the parametric surface:

$$S(u, v) = \frac{\sum_{j=0}^m \sum_{i=0}^n N_{i,p}(u) N_{j,q}(v) w_{i,j} \mathbf{d}_{i,j}}{\sum_{j=0}^m \sum_{i=0}^n N_{i,p}(u) N_{j,q}(v) w_{i,j}} \quad 0 \leq u, v \leq 1. \quad (13)$$

From the above mentioned set of NURBS curves, an approximated NURBS surface (the yellow surface in Figure 2b) is then generated via a lofting technique described in [14]. At this step, the original backdoor geometry is approximated by the obtained NURBS surface, which can be fully described by the given control points.

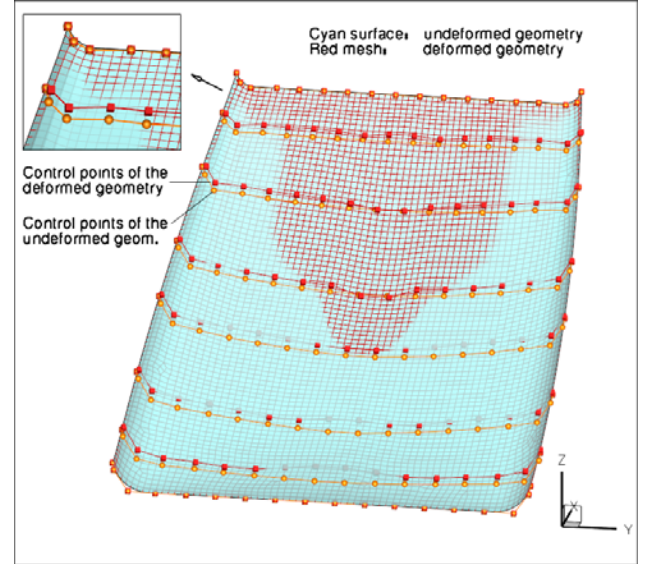


Figure 3: Surface deformation of the backdoor geometry.

Except the control points on the boundary curves, which should be kept unchanged for the reason of geometrical continuity, the rest of the control points are used for the shape modification. For symmetry reason only the 48 control points on the left side (marked with red circles in Figure 2b) are actually used for the shape modification, then their deflections are mirrored to the control points on the right side. Within the current study, only the x- and the z-coordinates of the control points are modified, therefore, a total number of 96 design variables are used for the optimization study. Note, with such a large number of design variables only gradient-based optimization is viable, and only the adjoint method can deliver the gradient efficiently.

The surface deformation by the deflection of the control points is demonstrated in Figure 3. The orange points are identical to the control points in Figure 2b, while the red points are the deflected control points according to the optimizer directives. In this way, a deformed backdoor geometry is obtained. The surface deformation of the backdoor is introduced into the computational domain by a mesh deformation technique based on RBF [7]. The basic idea is to apply an interpolation function for the surface deformation to the nodes of the volume mesh, with a superimposed blending function based on the wall distance of the nodes, so that the mesh quality within a certain wall distance can be maintained (see Figure 4). This feature is important for the comparison of the numerical results, since the mesh resolutions of the boundary layers between different meshes must be preserved.

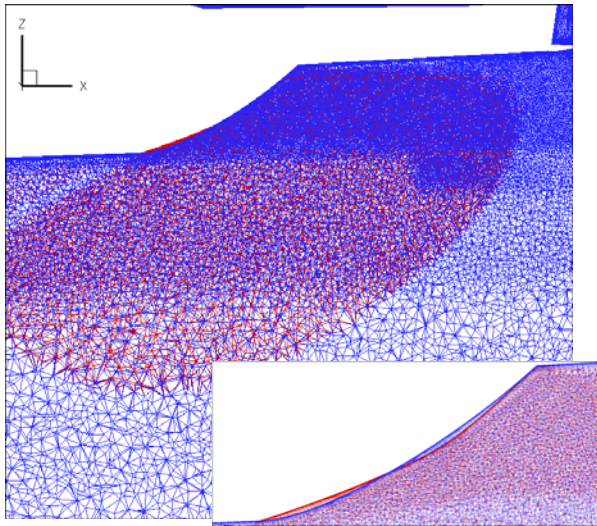


Figure 4: Volume mesh deformation based on RBF (The Meshes are cut at  $y=0$ . Blue: original mesh, Red: deformed mesh).

## 2.5. Computational Setup

The above described optimization process chain has been applied to a modified GOAHEAD [1] geometry, and a cruise flight condition at Sea Level ISA (defined within the GRC2 project of Clean Sky JTI) is considered (see Table 1).

For the analysis of the flow field around the backdoor area, the influence of the geometry details on the upper fuselage side was found in preliminary tests to be marginal for an angle of incidence  $\alpha = -2^\circ$ . For this reason, the rotor mast cowl and the exhaust nozzles of the GOAHEAD configuration were not considered here. No further modifications of the geometry have been performed.

Parameter	Symbol	Unit	
Free stream air speed	$U_\infty$	m/s	70
Pressure	$P_\infty$	Pa	101325
Density	$\rho_\infty$	kg/m <sup>3</sup>	1.225
Temperature	$T_\infty$	K	288
Angle of attack	$\alpha$	Deg	-2
Sideslip angle	$\beta$	Deg	0
Free stream Reynolds number	$Re$	1/m	$4.79 \times 10^6$
Free stream Mach number	$Ma$	-	0.206

Table 1: Simulation parameters.

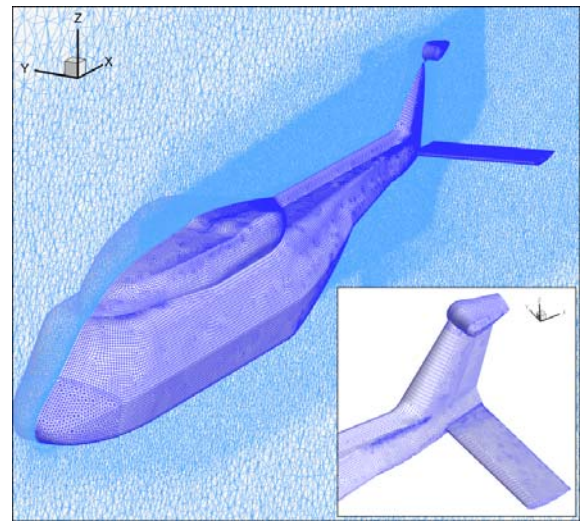


Figure 5: Overview of the grid setup.

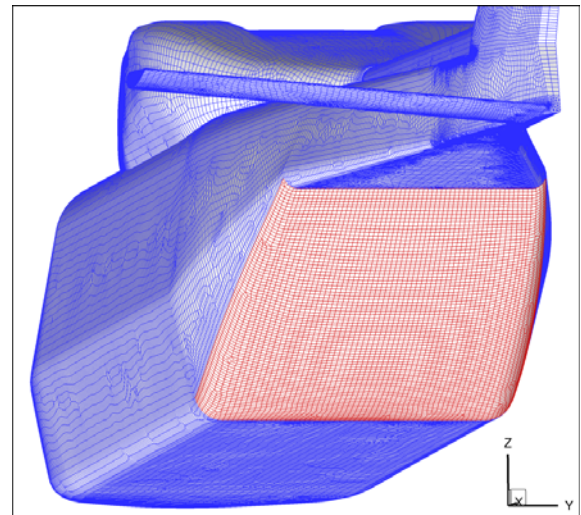


Figure 6: Surface mesh of the backdoor area.

The unstructured grid used for the present study has been generated with the hybrid grid generation software CENTAUR from CENTAUROsoft [15].

Quadrilateral elements for the surface and hexahedral elements for the boundary layer resolution were more preferred than triangles and prisms during the mesh generation, since in general they allow higher aspect ratios while maintaining or even reducing discretization errors. On the backdoor surface, structured hexahedral layers were mostly used.

The first cell height is set to be 0.005 mm and the far field boundary is a sphere with a radius of 20 times of the fuselage length (ca. 80 m). The computational mesh has a total node number of  $5.73 \times 10^6$  and is shown in Figure 5 and Figure 6. Only the red coloured mesh in Figure 6 was deformed during the optimization study.

### 3. RESULTS AND DISCUSSIONS

For the optimization study, the cost function is selected to be the total drag coefficient  $C_D$  of the helicopter configuration, which is  $C_{D,orig} = 5.169 \times 10^{-2}$  for the original geometry. In this paper, the drag and lift coefficient are obtained from pressure and skin-friction integration on the fuselage surface and the reference area is  $1 \text{ m}^2$ . The history of the  $C_D$  during the design process is plotted in Figure 7. After 12 function evaluations (i.e., flow simulations) and two times of solving the adjoint equations, an local minimum at  $C_{D,opt} = 5.058 \times 10^{-2}$  was found. In the last cycle of the optimization run, the objective can not be improved further. The reason is that the line search algorithm is very sensitive to small inaccuracy in the gradient calculation in the near of a local minimum. Nevertheless, a total drag reduction of 2.15% could be achieved, which corresponds to about 11 drag counts. As can be seen in Figure 7, the lift coefficient  $C_L$  is increased during the optimization which is favourable from the view of aerodynamic design. The reason for this effect will be explained later in this section. In the following the flow field around the original and the optimized backdoor geometry, which is the geometry after the second design cycle, will be compared and discussed.

In Figure 9 the contours of the skin friction coefficient  $C_f$  on the original and the optimized geometries are compared with each other. It can be easily seen that the region of separated flow is reduced on the optimized backdoor geometry. A look on the optimized backdoor geometry (see Figure 10a) shows that a bump is generated ahead the flow separation region, which is the reason for the delay of the separation line. On the bottom of the backdoor, the geometry is deformed inward. The displacement of the surface mesh nodes is plotted in Figure 10b. The maximal node displacement on the

backdoor is about 20 cm. As also can be seen in Figure 4 (the red mesh is the computational mesh of the optimized backdoor geometry), the optimizer effectively streamlined the backdoor shape on the symmetry plane at  $y=0$ .

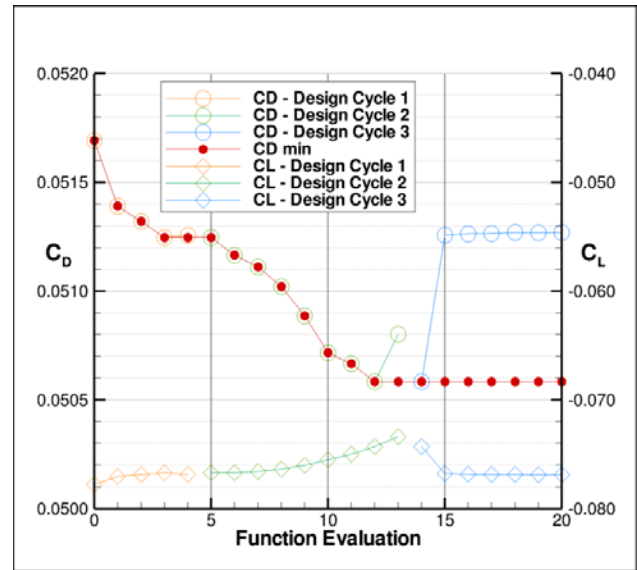
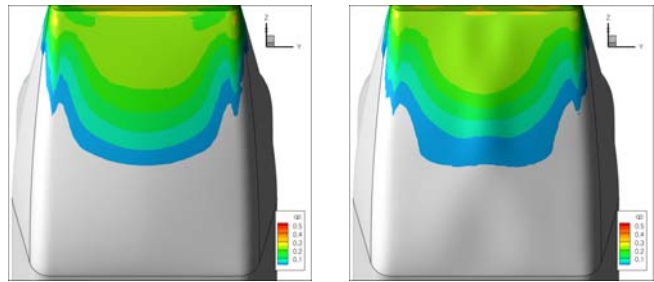


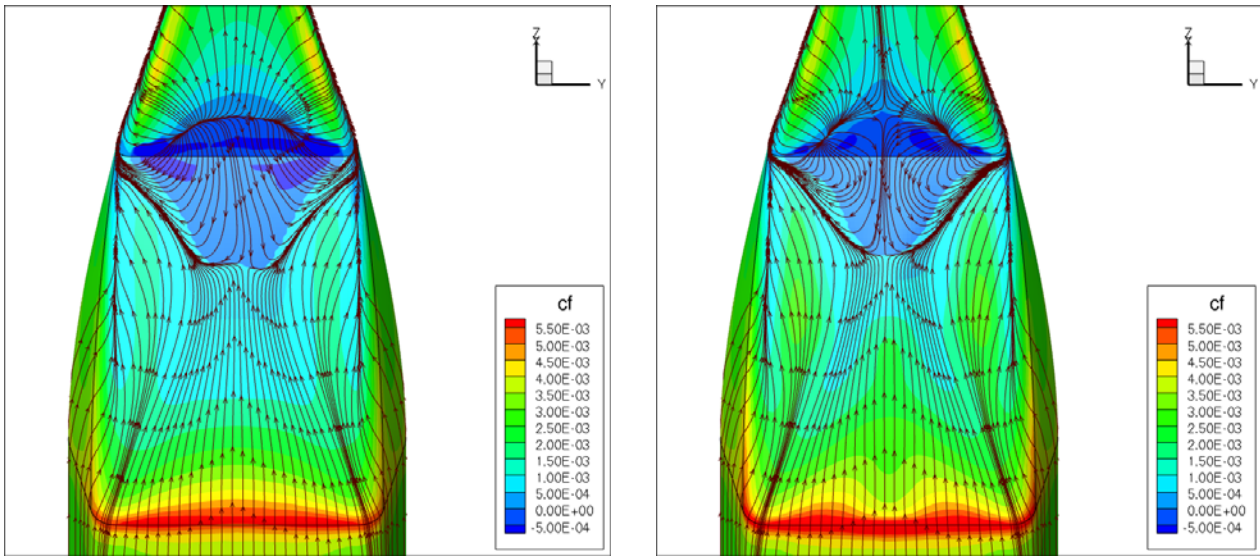
Figure 7: Time history of  $C_D$  and  $C_L$  during the optimization process.



(a) Original geometry (b) Optimized geometry

Figure 8: Comparison of the pressure patterns on backdoor.

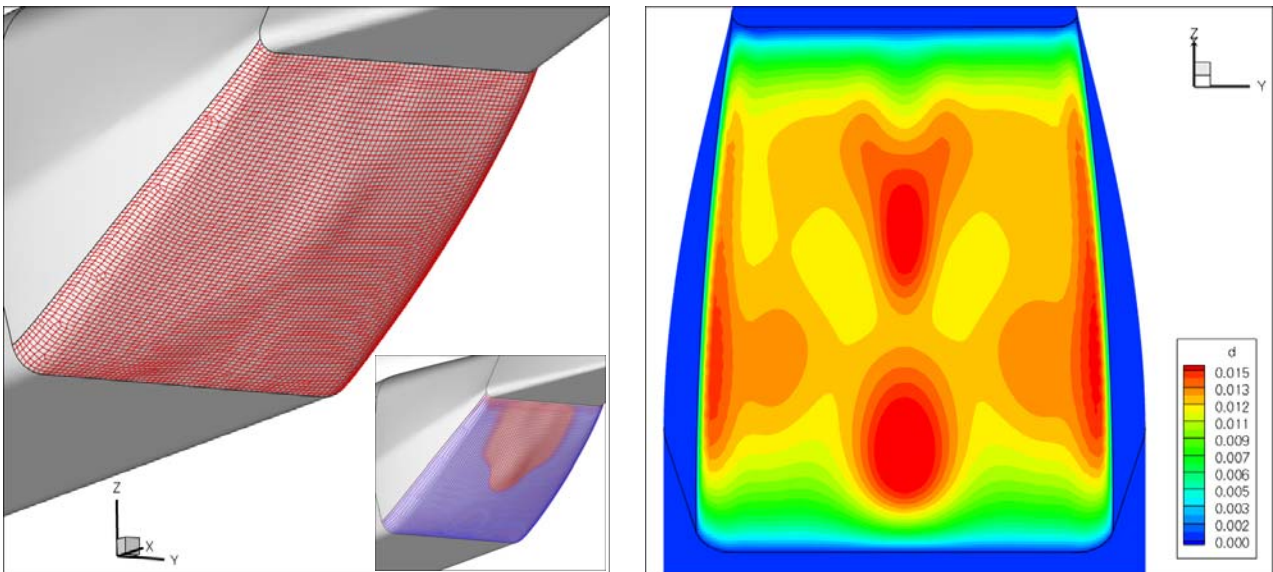
On the backdoor, the areas with pressure value above the static pressure (i.e.  $C_p > 0$ ) produce a force component in the flight direction, which is equivalent with the reduction of the pressure drag. These areas on the backdoor are shown in Figure 8 by switching off the areas with negative  $C_p$  values. They are related to the ability of the configuration for the pressure recovery, and therefore can be used for the visual assessment of drag reduction. It shows that the area with positive  $C_p$  is increased on the optimized backdoor geometry (Figure 8b). Due to the upsweep angle of the tail, the increase of the static pressure on the backdoor also produces a force component in the upper direction, which contributes to the increase of the lift coefficient (see Figure 7).



(a) Original geometry

(b) Optimized geometry

Figure 9: Contour plots of the skin friction coefficient and surface stream lines.



(a) Optimized geometry:  
Red: optimized, Blue: original

(b) Magnitude of the displacement of the surface mesh nodes.

Figure 10: Result of the optimized backdoor shape.

A drag breakdown analysis has been performed to find the origin of the drag reduction. In Figure 11, only the  $C_D$  values of the backdoor and its neighbouring parts before and after the optimization are summarized, since the  $C_D$  values of other fuselage components are nearly unchanged. The total drag coefficient of the backdoor surface is reduced from  $7.176 \times 10^{-3}$  to  $6.030 \times 10^{-3}$ , i.e., a drag reduction of about 16% locally. In the lower part of Figure 11, the local change of  $C_D$  is normalized with the total drag coefficient of the original geometry  $C_{D,orig}$ . It shows that the major source of the drag reduction results as expected from the backdoor area.

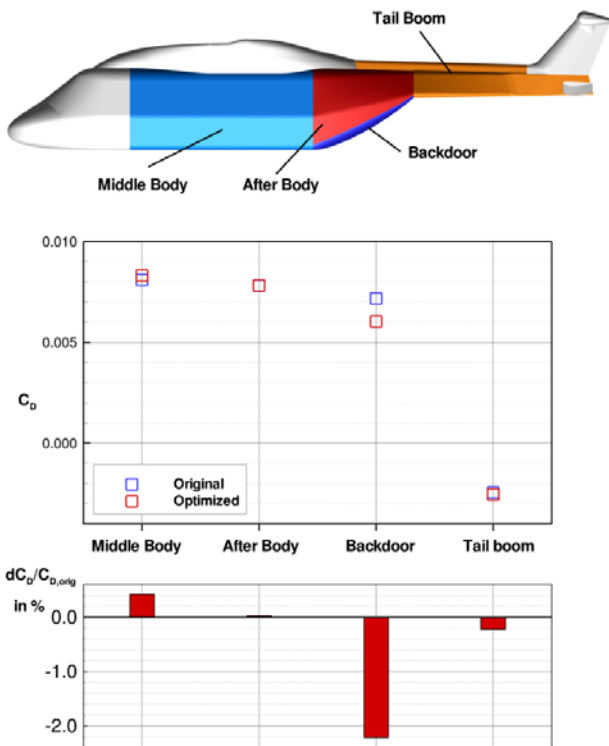
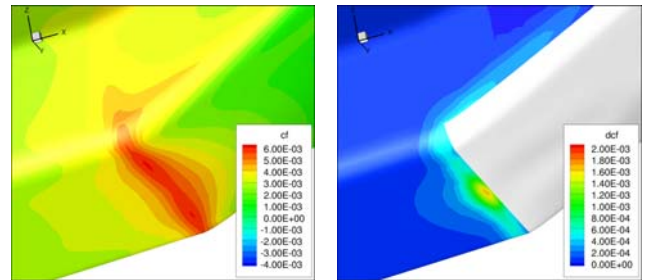


Figure 11: Change of  $C_D$  values on the backdoor and in the neighbouring regions.

The small drag increase on the middle body of the fuselage has its origin in the skin friction distribution, as shown in Figure 12. The backdoor geometry is deformed inward at the bottom, which leads to a local increase of the velocity. This effect increases the local skin friction on the middle body, as depicted in Figure 12b (the  $C_f$  difference are calculated on a node to node basis, therefore, the differences on the deformed backdoor is not shown here, since it would be not directly comparable).

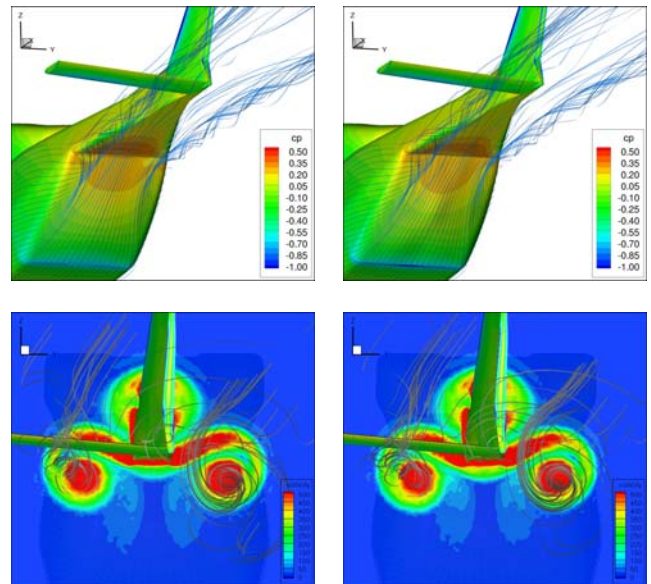
The up-rolling vortices from the upswept tail of an aircraft are another major source of drag production. A comparison of the stream lines and the vorticity magnitude behind the original and the optimized configuration (Figure 13) shows that the strengths of

the up-rolling vortices can only be reduced slightly through the backdoor shape optimization. The strength of such vortices can be efficiently reduced using optimal placed tail strakes which will be a subject of future investigations.



(a) Original geometry (b) Optimized geometry

Figure 12: Comparison of the  $C_f$  patterns on the middle body.



(a) Original geometry (b) Optimized geometry

Figure 13: Comparison of the wake behind the original and the optimized configurations.

#### 4. CONCLUSIONS

In this paper, an automatic optimization chain for a modified GOAHEAD helicopter configuration has been presented. The optimization chain is implemented with the Python language and consists of calls to several external programs and tools, such as a CFD solver, a solver for the adjoint equations, surface parameterization and mesh deformation tools. In the current study, the total drag of the helicopter configuration under a cruise flight

condition could be reduced by 2.15% via local shape modification on the backdoor geometry. The main source and the mechanism for the drag reduction could be identified and understood. These first results of the optimization study clearly demonstrated the applicability of the established optimization method.

Nevertheless, since the flow field around a helicopter is extreme complex and difficult to predict, further investigations concerning the accuracy of the CFD calculation must be performed. In a next step, it would be a further challenge to carry out the optimization studies under more realistic conditions, for instances, taking the structural constraints into account.

## REFERENCES

- [1] Pahlke, K.: The GOAHEAD Project. 33rd European Rotorcraft Forum, Kazan, Russia, 2007.
- [2] Keys, C., Wiesner R.: Guidelines for Reducing Helicopter Parasite Drag, J. Am Helicopter Society, Vol. 20, pp.31-40, 1975
- [3] Jameson A.: Aerodynamics Design via Control Theory, J. of Scientific Computing, Vol. 3, pp. 233-260, 1988.
- [4] A. Jameson and L. Martinelli: Aerodynamic Shape Optimization Techniques Based on Control Theory, CIME (International Mathematical Summer Center), Martina Franca, Italy, 1999.
- [5] Dwight, R.P.: Efficiency Improvements of RANS-Based Analysis and Optimization using Implicit and Adjoint Methods on Unstructured Grids, Ph.D. thesis, University of Manchester, Manchester, UK, 2006.
- [6] Brezillon, J., Dwight, R.: Aerodynamic Shape Optimization using the Discrete Adjoint of the Navier-Stokes Equations: Applications towards Complex 3D Configurations, Proceedings of the CEAS/KATnet II Conference on Key Aerodynamic Technologies, Paper No. 36-1, May 2009.
- [7] Heinrich, R., Kroll, N., Neumann, J., Nagel, B.: Fluid - Structure Coupling for Aerodynamic Analysis and Design – A DLR Perspective, 46th AIAA Aerospace Sciences Meeting and Exhibit 2008, AIAA Paper 2008-056, Reno, USA, 2008.
- [8] Spalart, P., Allmaras, S.: A One-Equation Turbulence Model for Aerodynamic Flows, AIAA Paper 92-0439, 1992.
- [9] Gerhold, T.: Overview of the Hybrid RANS Code TAU, MEGAFLOW – Numerical Flow Simulation for Aircraft Design, edited by N. Kroll and J. Fassbender, Vol. 89 of Notes on Numerical Fluid Mechanics and Multidisciplinary Design, Springer, pp. 81-92, 2005
- [10] Schwamborn, D., Gerhold, T., Heinrich, R.: The DLR TAU-Code: Recent Applications in Research and Industry, Proceedings of ECCOMAS CFD 2006, Delft, Netherland, 2006.
- [11] Fletcher, R., Reeves, C.M.: Function Minimization by Conjugate Gradient, Computer J., 7, 149-154, 1964.
- [12] Cox, M.G.: The numerical evaluation of B-Splines. The Institute of Mathematics and its Applications, Vol. 10, pp. 134-149, 1972.
- [13] Hoschek, J., Lasser, D.: Fundamentals of Computer Aided Geometric Design, 1. Edition, AK Peters, 1993
- [14] Piegl, L., Tiller, W.: The NURBS Book, Springer, Berlin, 1996.
- [15] CENTAURSoft: <http://www.centaursoft.com>